Rotationally Resolved Photoelectron Angular Distributions from a Nonlinear Polyatomic Molecule

Paul Hockett, Michael Staniforth, and Katharine L. Reid
School of Chemistry, University of Nottingham, Nottingham NG7 2RD, United Kingdom

Dave Townsend
School of Engineering and Physical Sciences, Heriot-Watt University, Edinburgh, EH14 4AS, United Kingdom
(Received 10 March 2009; published 24 June 2009)

We present, for the first time, rotationally resolved photoelectron images resulting from the ionization of a polyatomic molecule. Photoelectron angular distributions pertaining to the formation of individual rotational levels of NH_3^+ have been extracted from the images and analyzed to enable a complete determination of the radial dipole matrix elements and relative phases that describe the ionization dynamics. This determination leads to the deduction of significantly different dynamics from those extracted in previous studies which lacked either angular information or rotational resolution.

DOI: 10.1103/PhysRevLett.102.253002 PACS numbers: 33.80.Rv, 33.60.+q, 33.80.Eh

Photoelectron angular distributions (PADs) are interference patterns, the position of whose lobes and nodes are determined by phase differences between the asymptotic scattering partial waves needed to express the photoelectron wave function [1]. For this reason, PADs are crucial probes of photoionization dynamics [2]. Because the number of scattering partial waves describing these dynamics increases with the complexity of the target that is ionized, a complete determination of the photoionization dynamics of a polyatomic molecule requires that PADs associated with a variety of experimentally controlled variables should be measured. One way of achieving this is to measure PADs for defined vibrational and rotational states of the polyatomic ion that is formed; an alternative is to measure PADs in a frame defined by the molecule. Both of these options present significant experimental challenges. The former requires an energy resolution that is beyond the limits of most techniques used in photoelectron spectroscopy, with the exception of the threshold method known as ZEKE which precludes the measurement of PADs. To date, PADs associated with resolved ion rotational states have only been measured for the diatomic molecules H_2 and NO [3]. The latter option requires a means of fixing the molecular frame with respect to the lab which has typically been achieved by the detection of a fragment ion in coincidence with the emitted photoelectron, limiting the systems that can be studied. This method has enabled the determination of the photoionization dynamics of various diatomic molecules [4], and linear triatomic molecules such as CS_2 [5].

In recent years, the technique of velocity map imaging (VMI) of photoelectrons [6] has gained popularity as an efficient method by which some ion internal state resolution is possible along with a simultaneous measurement of the associated PADs [7]. Although it has been shown that the energy resolution of this technique improves as photoelectron kinetic energy is reduced [8], rotational resolution of a polyatomic ion has not been demonstrated to date. Despite this, a VMI study allowed the determination of the photoionization dynamics of the linear polyatomic molecule acetylene owing to the operation of strict symmetry selection rules which restricted the possible dynamical pathways [9]. For nonlinear polyatomic molecules, such restrictions will be less severe or absent, and rotational resolution is required unless approximations are made [10].

Ammonia (NH_3) is pyramidal in its $\tilde{X}\ ^1A_1''$ ground electronic state, but planar in the ground electronic state of the ion and in the Rydberg states that converge on it. This enables a Rydberg state to be prepared on excitation from the vibrationless ground state which has significant quanta, υ_2, in the ν_2 "umbrella" vibrational mode. In the work presented here, the $\tilde{B}\ ^1E''$ (predominantly $p\pi$ Rydberg state) is prepared with four quanta in this vibrational mode, and various selected rotational levels, using two photons from a nanosecond laser beam at ~315 nm. The rotational levels are denoted N_K, where N is the rotational angular momentum quantum number and K denotes its projection on the C_3 molecular axis. Several probe (ionization) wavelengths were used; here, we present results at 431.3 nm which allows the formation of the NH_3^+ ion in rotational levels associated with the $\Delta\upsilon_2 = 0$ transition, creating photoelectrons with kinetic energies up to ~300 cm^{-1} (0.037 eV).

Our VMI spectrometer follows the now standard Eppink and Parker design [6], and has been described in detail elsewhere [11]. A 10% mixture of ammonia in argon was introduced into the spectrometer via a pulsed nozzle [11]. Photoelectrons were focused by an electrostatic lens onto a position sensitive detector comprising two microchannel plates and a phosphor screen. The electrostatic lens voltages were −160 V (repeller) and −108 V (extractor), chosen to expand the photoelectron clouds resulting from the $(2 + 1')$ ionization process so that they filled the detector, at the expense of those photoelectrons resulting

from (2 + 1) ionization which fell beyond the edges of the detector.

In Figs. 1(a) and 1(b), we show photoelectron images following the excitation of ammonia from its $N_K = 1_1$ rotational level in the $\tilde{X}\ ^1A_1''$ state to the $N_K = 3_2$ and 2_2 rotational levels in the $\tilde{B}\ ^1E''$ state, respectively, and ionization with 431.3 nm. The images were analyzed using the pBasex inversion method [12] to give photoelectron kinetic energy and angular distributions. The distributions thus extracted from the images shown in Fig. 1 are shown in Figs. 2 and 3. The peaks in the photoelectron kinetic energy distribution shown in Fig. 2 can be assigned to N_K levels of the NH_3^+ ion, as labeled in Figs. 2 and 3, by comparison with previous work in the literature [13,14].

A detailed comparison can be made with two earlier studies in which ammonia was ionized following excitation to the $\tilde{B}\ ^1E''$ state [15,16]. In these studies, threshold ionization was used enabling excellent energy resolution but no angular information. In the work published by Softley and coworkers [16], multichannel quantum defect calculations were also used to analyze the observed ion rotational state distributions. The use of field ionization in both of these studies, and the fact that extracted electrons were born with zero kinetic energy, may mean that the recorded spectra were susceptible to different ionization dynamics from those observed here. Nonetheless, it is instructive to compare the ion rotational state distributions with the ones measured here. Strict parity selection rules govern the ion states that are formed. The transitions studied here all involve *para*-NH_3, which means that the formation of NH_3^+ with $K = 0$ or 3, which would be *ortho*, is forbidden. In addition, odd-l photoelectron partial waves are associated with the formation of ion states with $K = 2$, 4 and even-l with $K = 1$, 5 [17].

Beyond these selection rules, a strong propensity is observed for those transitions with $\Delta N = 0, \pm 1$, $\Delta K = \pm 1$, where ΔN is the change in N on ionization from the selected $\tilde{B}\ ^1E''$ state level, and ΔK is the corresponding change in K. This is consistent with the assignment of the $\tilde{B}\ ^1E''$ state as predominantly a $p\pi$ Rydberg state that obeys atomiclike selection rules [16], i.e., a propensity for the formation of photoelectron partial waves with $l = 0, 2$. Less intense features that can be explained by atomiclike selection rules originating from the minority $d\delta$ contribution to the $\tilde{B}\ ^1E''$ state [16] can also be seen in the spectra and give rise to rotational levels with $\Delta K = \pm 2$. Of particular interest is the population of ion rotational levels resulting from transitions with $\Delta N > 1$, $\Delta K = 1$ which cannot be explained by atomic selection rules. This includes the 1_1 and 5_1 levels [Fig. 2(a)] and the 4_1 level [Fig. 2(b)]. The breakdown of these selection rules reflects the rescattering of the photoelectron from the short-range, noncentral molecular potential, and the exchange of angular momentum between the outgoing electron and the ion core. These features are observed with different relative intensities in this work and in the two threshold ionization studies. For example, the 5_1 feature which is clearly visible in Fig. 2(a) is much smaller in Ref. [16] and not seen at all in Ref. [15]. In addition, the 3_1 feature (Fig. 2) is the most intense "atomiclike" line originating from the $p\pi$ Rydberg component in Ref. [16], but least intense in both our work and in Ref. [15].

Photoelectron angular distributions (PADs) associated with resolved NH_3^+ rotational states have not been measured before, although vibrationally resolved PADs have been measured corresponding to photoelectron kinetic energies of ~1 eV [10]. The PADs shown in Fig. 3 have significant anisotropy and are strikingly sensitive to ion rotational state. The fact that three photons are involved in the ionization process means that, providing cylindrical

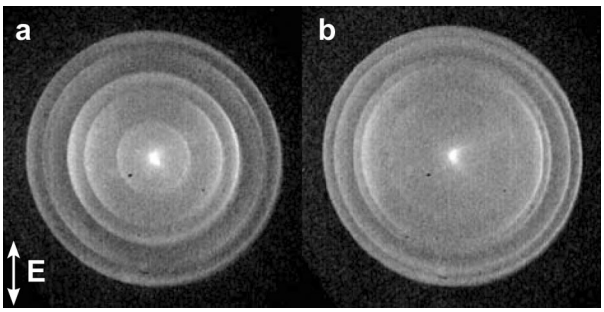

FIG. 1. Raw photoelectron images recorded via the (a) $1_1 \rightarrow 3_2$ (b) $1_1 \rightarrow 2_2$ pump transitions and a probe wavelength of 431.3 nm.

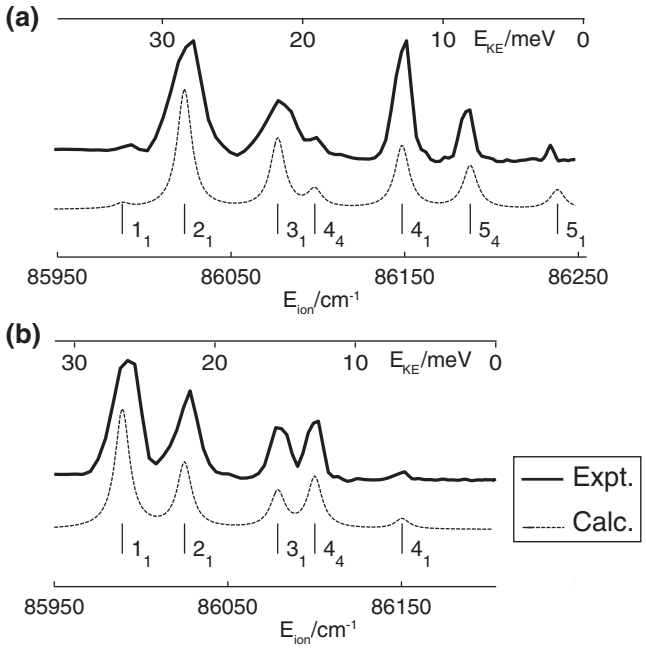

FIG. 2. Photoelectron spectra extracted from images recorded via the (a) $1_1 \rightarrow 3_2$ (b) $1_1 \rightarrow 2_2$ pump transitions (solid line). Corresponding simulated photoelectron spectra using rotational level positions based on the rotational constants taken from Ref. [13], and intensities derived from the β_{00} values calculated using the matrix elements listed in Table I (dashed line).

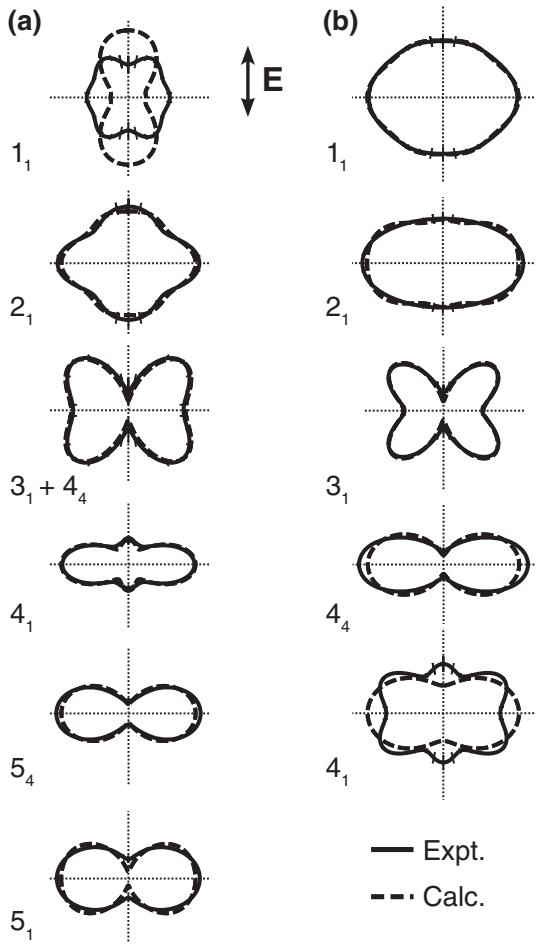

FIG. 3. Polar plots of photoelectron intensity according to Eq. (1) using the β_{LM} values extracted from the pBasex inversion of the images recorded via the (a) $1_1 \rightarrow 3_2$ (b) $1_1 \rightarrow 2_2$ pump transitions (solid line) and β_{LM} values calculated from the dipole matrix elements listed in Table I (dashed line). For plotting purposes, all PADs are normalized such that $\beta_{00} = 1$. Errors are derived from pBasex [12] during image analysis.

symmetry is maintained, the angle-resolved photoelectron intensity in the lab frame, $I(\theta, \phi)$, can be expressed as a sum of four terms:

$$I(\theta, \phi) = \beta_{00} Y_{00}(\theta, \phi) + \beta_{20} Y_{20}(\theta, \phi) + \beta_{40} Y_{40}(\theta, \phi) + \beta_{60} Y_{60}(\theta, \phi), \quad (1)$$

where the $Y_{LM}(\theta, \varphi)$ are spherical harmonic functions, and the β_{LM} coefficients are anisotropy parameters, with β_{00} giving the angle-integrated cross section. Significant β_{60} values are required to fit several of the PADs. Some of the PADs related to N_K levels in the ion which are only accessible via rescattering [1_1 in Fig. 3(a); 4_1 in Fig. 3(b)] show large β_{60} terms which dominate the PAD. Other PADs also have significant β_{60} values [e.g., 4_1 in Fig. 3(a)], but this contribution is less substantial in PADs that can be accounted for by "atomiclike" photoionization. The appearance of nonzero β_{60} terms requires the production of partial waves with orbital angular momentum $l \geq 3$ in the rescattering process, and if the ion rotational level has $K = 1$ or 5 then, from above, l must be even, and so g waves are required.

The extracted β_{LM} parameters can be fit to a model [9,10,18] that enables the determination of the magnitudes, $r_{l\lambda}$, and phases, $\eta_{l\lambda}$, of the radial dipole matrix elements connecting a given $\tilde{B}\ ^1E''$ state level to a given $l\lambda$ photoelectron partial wave. These matrix elements represent integrals over the internuclear coordinates according to the appropriate vibrational wave function and are expected to depend only weakly on photoelectron kinetic energy [19]. Therefore, it was possible to include PADs associated with ion rotational levels that were formed following six different $\tilde{X}\ ^1A_1''(v_2 = 0) \rightarrow \tilde{B}\ ^1E''(v_2 = 4)$ transitions ($1_1 \rightarrow 1_0,\ 2_0,\ 2_2,\ 3_2;\ 1_0 \rightarrow 1_1,\ 3_1$), giving 30 unique PADs in all, in a single fit. Fitting was performed in Matlab (R2006b) using the LSQCURVEFIT algorithm. The fit was intensity-weighted to allow for larger uncertainties in the extracted β_{LM} coefficients for PADs correlated with weaker features in the spectrum. The rotational branching ratios were not fitted directly, but can be simulated from the β_{00} values obtained from the fitted dipole matrix elements.

Fits of those PADs shown in Fig. 3 to the model are presented in the same figure as dashed lines, and the simulated spectra resulting from the rotational branching ratios predicted by the fit are shown underneath each relevant experimental spectrum in Fig. 2. From angular momentum coupling $\Delta N_{max} = l_{max} + 1$, so partial waves up to a maximum l of 3 are sufficient to account for all of the rotational peaks seen in the spectra. However, as discussed above, the presence of $l = 4$ is required to allow for the nonzero β_{60} contribution to some of the PADs correlated with odd K^+. This result is significant as previous studies of the photoionization dynamics of ammonia in its $\tilde{B}\ ^1E''$ state have excluded contributions from $l > 3$ [10,16]. It also illustrates that rotational branching ratios alone are insufficient to determine photoionization dynamics. As can be seen in the examples shown in Figs. 2 and 3, the final parameters reproduce both the PADs and rotational spectra very convincingly, especially for those rotational states that are expected to be formed in the atomic picture. Although the PADs associated with features which arise from rescattering, and the corresponding features in the rotational spectra, are not so well reproduced, the fit result is robust, and because of the intensity, weighting applied does not change significantly if the rescattering features are omitted altogether.

The final parameters and associated uncertainties are listed in Table I. The magnitudes $r_{l\lambda}$ are normalized such that the total cross section is unity. In this work only relative magnitudes can be determined because the absolute cross-section is not measured. Table I also lists $r_{l\lambda}^2$ values, the relative cross section for each $l\lambda$ component, and the relative l-wave cross section F_l. Relative phases are split into even-l and odd-l because there is no interference between the two continua. In each case, one phase is

TABLE I. Fitted magnitudes ($r_{l\lambda}$) and relative phases ($\eta_{l\lambda}$) of the radial dipole matrix elements for ionization with associated uncertainties. The $\eta_{l\lambda}$ values include the Coulomb phase shifts.

l	λ	$r_{l\lambda}$	$\eta_{l\lambda}$(deg)	$r_{l\lambda}^2$(%)	F_l(%)
s	σ	0.357(12)	0*	12.7(17)	12.7(17)
p	σ	⋯	⋯		13.0(11)
	π	0.361(8)	0*	13.0(11)	
d	σ	0.137(4)	31(9)	1.9(5)	53.0(7)
	π	0.387(2)	16(3)	15.0(3)	
	δ	0.601(3)	149(2)	36.1(4)	
f	σ	⋯			10.7(2)
	π	0.084(1)	162(3)	0.7(1)	
	δ	0.143(1)	153(1)	2.1(1)	
	ϕ	0.282(1)	153(1)	8.0(1)	
g	σ	0.171(7)	92(9)	2.9(10)	10.5(17)
	π	0.276(8)	64(23)	7.6(12)	
	δ	0.000(5)	⋯	0.0	
	ϕ	⋯	⋯		
	γ	⋯	⋯		

set to 0 as a reference phase, and the final results are quoted unsigned and mod (360°). The radial dipole matrix elements we have determined show a substantial d-wave contribution, but also a significant, and irrefutable, g-wave contribution (~10% of the overall photoelectron intensity) which has not been observed before [10,16], but is required to explain the observed anisotropies in the rotationally resolved PADs. Given the mixed $p\pi/d\delta$ character of the $\tilde{B}\ ^1E''$ Rydberg state, the g wave can only be caused by rescattering of the initially formed photoelectrons from the molecular potential, resulting in mixing of orbital angular momenta. There are also differences in the relative contribution of the λ components of each l wave; this cannot be explained by an atomic analogy.

Of particular interest are the deduced phase differences between partial waves, whose unambiguous experimental determination relies on the measurement of photoelectron angular distributions for resolved ion rotational states [2]. The relative phases, $\eta_{l\lambda}$, can in principle be predicted from the quantum defects, $\mu_{l\lambda}(n)$ at $n \rightarrow \infty$ [19] once the Coulomb phase has been subtracted. However, the quantum defects in ammonia have only been deduced from experiment for $n < 20$ in the s, p, and d Rydberg series [16]. The phases predicted from these values do not agree well with those resulting from our fit. Because we have measured PADs associated with *each* ion rotational level formed following six different $\tilde{X}\ ^1A_1''(v_2 = 0) \rightarrow \tilde{B}\ ^1E''(v_2 = 4)$ transitions, we have confidence in the uniqueness of the determined values of our radial dipole matrix elements and phases (Table I), as corroborated by extensive mapping of the χ^2 hypersurface probed by our fit. In earlier work [10,16], in which fewer experimental data points were obtained, the available values of the quantum defects were used directly to fit the data. Our results lead us to conclude that this gives an incorrect picture.

In conclusion, we have shown that resolution of ion rotational states combined with the measurement of photoelectron angular distributions has enabled the first complete determination of the radial dipole matrix elements and relative phases that describe the photoionization dynamics of a nonlinear polyatomic molecule. Significant rescattering of the photoelectron, in particular into the g-wave continuum channel, is invoked to explain the anisotropies observed for photoionization of $NH_3(\tilde{B}\ ^1E'')$; this is supported by the fit to our data and differs significantly from the conclusions of earlier studies. Finally, we note that the use of an appropriate ionization wavelength allows the rotational resolution of small polyatomic ions to be achieved with photoelectron imaging.

[1] H. Bethe and E. Salpeter, *Quantum Mechanics of One- and Two-Electron Atoms* (Academic Press Inc., Berlin, 1957).

[2] J. Cooper and R. N. Zare, J. Chem. Phys. **48**, 942 (1968); S. J. Smith and G. Leuchs, Adv. At. Mol. Phys. **24**, 157 (1988); D. Dill, J. Chem. Phys. **65**, 1130 (1976); K. L. Reid, Annu. Rev. Phys. Chem. **54**, 397 (2003).

[3] S. L. Anderson, G. D. Kubiak, and R. N. Zare, Chem. Phys. Lett. **105**, 22 (1984); G. Ohrwall and P. Baltzer, Phys. Rev. A **58**, 1960 (1998); D. J. Leahy, K. L. Reid, and R. N. Zare, J. Chem. Phys. **95**, 1757 (1991); H. Park and R. N. Zare, J. Chem. Phys. **104**, 4568 (1996).

[4] O. Gessner *et al.*, Phys. Rev. Lett. **88**, 193002 (2002); S. Motoki *et al.*, Phys. Rev. Lett. **88**, 063003 (2002); M. Lebech *et al.*, J. Chem. Phys. **118**, 9653 (2003).

[5] T. Teramoto *et al.*, J. Phys. B **40**, 4033 (2007).

[6] A. T. J. B. Eppink and D. H. Parker, Rev. Sci. Instrum. **68**, 3477 (1997).

[7] T. Suzuki, Annu. Rev. Phys. Chem. **57**, 555 (2006); B. J. Whitaker, *Imaging in Molecular Dynamics: Technology and Applications* (Cambridge University Press, Cambridge, 2003).

[8] A. Osterwalder *et al.*, J. Chem. Phys. **121**, 6317 (2004).

[9] P. Hockett and K. L. Reid, J. Chem. Phys. **127**, 154308 (2007).

[10] D. Townsend and K. L. Reid, J. Chem. Phys. **112**, 9783 (2000).

[11] S. M. Bellm and K. L. Reid, Chem. Phys. Lett. **395**, 253 (2004).

[12] G. A. Garcia, L. Nahon, and I. Powis, Rev. Sci. Instrum. **75**, 4989 (2004).

[13] G. Reiser, W. Habenicht, and K. Mueller Dethlefs, J. Chem. Phys. **98**, 8462 (1993).

[14] R. Seiler *et al.*, J. Chem. Phys. **118**, 10024 (2003).

[15] W. Habenicht, G. Reiser, and K. Mueller Dethlefs, J. Chem. Phys. **95**, 4809 (1991).

[16] H. Dickinson, D. Rolland, and T. P. Softley, J. Phys. Chem. A **105**, 5590 (2001).

[17] R. Signorell and F. Merkt, Mol. Phys. **92**, 793 (1997).

[18] S. N. Dixit and V. McKoy, J. Chem. Phys. **82**, 3546 (1985).

[19] H. Park and R. N. Zare, J. Chem. Phys. **104**, 4554 (1996).